BI-DIRECTIONAL LOADING TESTS ON RC SHEAR WALLS SUBJECTED TO VARYING AXIAL LOAD

YAMADA Ryo[1], TANI Masanori[2], NISHIYAMA Minehiro[3]

SUMMARY

This paper reports loading tests conducted to investigate the effect of tri-directional seismic force on the shear capacity of RC shear walls. The experimental parameters were magnitude of out-of-plane deformation and axial load condition. One specimen was subjected to constant axial load, and the other three specimens were subjected to varying axial load. All specimens reached the in-plane maximum load capacity around R_x=0.50%, and after the maximum load capacity point, the loading capacity decreased due to shear failure. The maximum value of the average shear stress divided by tensile strength of concrete decreased with increasing difference between axial compressive force and tensile force.

***Keywords**: Bi-directional lateral loading; Shear failure; Shear wall; Varying axial load*

INTRODUCTION

Barbell-shaped shear walls, which have columns on the sides, are often utilized to enhance seismic resistance of buildings in Japan. Shear walls are subjected to in-plane shear force as well as out-of-plane shear force during earthquakes. In addition, the shear walls that are arranged in the gable part of buildings are subjected to varying axial load, so they are supposed to be subjected to tri-directional loading. However, the effect of tri-directional loading on shear capacity is not considered in practical structural design. Barbell-shaped shear walls have side columns as boundary elements, which may be damaged by out-of-plane forces during an earthquake. In consequence, it is expected that the in-plane shear capacity should decrease. In the shaking table test of a 6-story RC building, which was designed according to the current building law and regulations in Japan, and its finite element analysis (Sugimoto et al., 2017 and Yonezawa et al., 2018), the maximum load capacities of shear walls in the first story were lower than those calculated according to a design equation (1), which is referred to in practical structural design in Japan.

$$Q_{su} = \left\{ \frac{0.068 p_{te}^{0.23} (F_c + 18)}{\sqrt{M / QD + 0.12}} + 0.85\sqrt{\sigma_{wy} p_{wh}} + 0.1\sigma_0 \right\} t_e j \quad (1)$$

where
Q_{su} = in-plane ultimate shear capacity of a shear wall [N];
p_{te} = equivalent ratio of tensile reinforcements [%] (=100a_t/t_{ed});
F_c = compressive strength of concrete [MPa];
M/Q = shear span [mm];

[1] *Graduate Student, Department of Architecture and Architectural Engineering, Kyoto University, Japan, e-mail: rc.yamada@archi.kyoto-u.ac.jp*
[2] *Associate Professor, Department of Architecture and Architectural Engineering, Kyoto University, Japan, e-mail: tani@archi.kyoto-u.ac.jp*
[3] *Professor, Department of Architecture and Architectural Engineering, Kyoto University, Japan, e-mail: mn@archi.kyoto-u.ac.jp*

This paper is a shortened version of a paper by the authors, which is shown below.
R. Yamada, M. Tani, M. Nishiyama (2022), "Tri-Directional Loading Tests on Reinforced Concrete Shear Walls," *ACI Structural Journal*, Vol. 119, No.5, pp.129-140.

D = total length of a shear wall including side columns [mm];
σ_{wy} = yield strength of horizontal reinforcement [MPa];
p_{wh} = horizontal reinforcement ratio;
σ_0 = average longitudinal stress to gross area of a shear wall [MPa];
t_e = equivalent width of a shear wall (gross area divided by D, not exceeding 1.5 times width of wall panel) [mm];
$j = 7d/8$ [mm];
$d = D\text{-}D_c/2$; and
$1 \leq M/QD \leq 3$.

The database of loading tests on shear walls with side columns without opening revealed that the average ratio of the maximum load capacities experimentally obtained to the calculated values using Equation (1) is 1.4 (Kusunoki et al., 2019). The minimum ratio estimated in the shaking table test, however, was 0.80. The shear forces applied on the members were obtained from FE analysis. Furthermore, the shear walls were subjected to bi-directional loading, and the axial load varied from tension to high compression. Therefore, the effect of tri-directional loading should be taken into account in structural design.

Bi-directional lateral loading tests on shear walls have been conducted by Beyer (2008) and Niroomandi (2018), for example. The effect of out-of-plane loading on in-plane capacity of barbell-shaped shear walls has been often discussed by researchers based on their experimental investigations. Idosako et al. (2017), for example, reported that the maximum shear capacity of the specimens subjected to bi-directional lateral loading decreased by not more than 18% compared with the in-plane loaded specimens.

On the other hand, many experiments with axial load ratios as a parameter have been performed (e.g., Kawai et al., 2016). However, there are very few studies including high compressive axial force and/or tensile axial force. Furthermore, no experimental studies are available dealing with the effect of bi-directional lateral loading and varying axial force simultaneously.

In conclusion, the seismic performance of shear walls in actual buildings has not been properly understood. This paper reports results of bi-directional lateral loading tests on shear wall specimens subjected to varying axial load. The tests were conducted to assess the behavior of shear walls subjected to tri-directional loading. Test parameters investigated in this study were O/I drift ratio (to be explained later) and axial load condition. The specimens were barbell-shaped shear walls, which are frequently designed and utilized in Japan. The maximum load capacity under tri-directional loading was studied with design equations in Japan based on the experimental results.

OUTLINE OF EXPERIMENT

Specimen Details

Four identical shear wall specimens with the same dimensions and reinforcement arrangements were constructed. The specimens were 30%-scaled shear walls. The specimen characteristics and the material properties are shown in Figs. 1 and 2, and Tables 1 - 3. The reported material properties were the average obtained from three 100 x 200 mm concrete cylinders tested on the first day of loading. The specimens had side columns (depth: 250 mm, width: 250 mm) and the distance between centers of the side columns was 1800mm. The width of the wall panel was 70 mm. The target compressive strength of concrete was 29 MPa. High strength rebars whose nominal yield strength was 785 MPa were utilized for the hoops in the side columns to increase out-of-plane shear strength. Each specimen was constructed with two concrete placements. The first placement was for the foundation, and its top surface was roughened with metal-bristle brushes. The second was for the test region and the top block several days later.

Table 1. Specimens characteristics

Part	Dimension(mm)	Arrangement of reinforcement			Grade	Reinforcement ratio (%)
Columns	250×250	Longitudinal reinforcement		10-D16	SD345	3.18
		Hoops	In-plane	4-S6@75	KSS785	0.68
			Out-of-plane	6-S6@75		1.01
Wall	1550×70	Vertical reinforcement		D6@150	SD295A	0.30
		Horizontal reinforcement				

Table 2. Material properties of concrete

Specimen	Compressive strength f'_c (MPa)	Tensile splitting strength f_t, (MPa)	Young's modulus E_c^* (GPa)
WB15-C20	21.9	3.55	17.1
WB15-C20T00	23.0	2.49	20.8
WB15-C20T33	26.9	2.22	22.3
WB30-C20T00	24.5	2.60	21.1
Grout for repairing	53.6	2.59	11.8

* f'_c /3 secant modulus

Table 3. Material properties of reinforcements

	D6	D16	S6
Yield strength (MPa)	474.1	381.0	866.9
Tensile strength (MPa)	536.1	549.7	979.7
Elastic modulus (GPa)	198.2	185.6	194.1

*0.2% offset stress

Table 4. Experimental parameters

Specimen	O/I drift ratio	Minimum axial load ratio	Service load ratio	Maximum axial load ratio
WB15-C20	1.5	0.20 (Constant)		
WB15-C20T00		0	0.12	0.20
WB15-C20T33		-0.33		
WB30-C20T00	3.0	0		

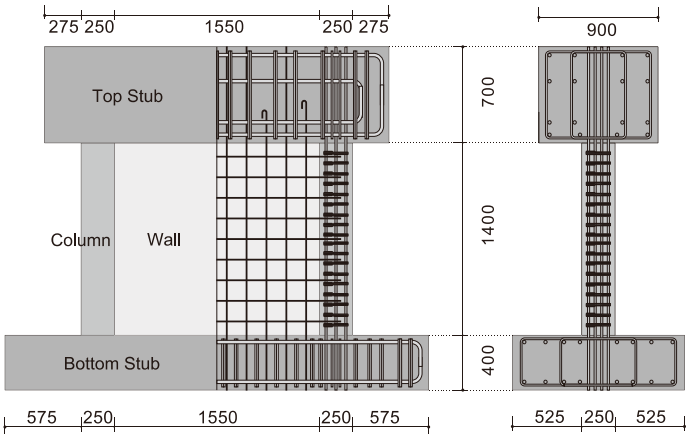

Figure 1. Dimensions of specimen (unit: mm)

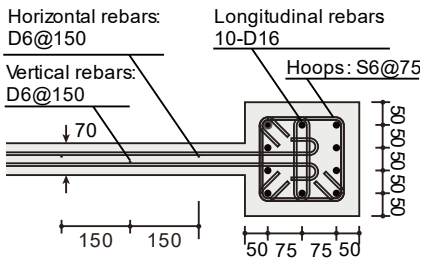

Figure 2. Cross section of test region (unit: mm)

Experimental Parameters

Parameters in the experiment are the ratio of out-of-plane drift to in-plane drift (O/I drift ratio) and the type of axial load. In this paper, axial load ratio means the ratio of axial load to the product of the gross area of the shear wall and concrete compressive strength when the axial load is in compression, and the ratio of axial load to the yield load of the longitudinal reinforcements in the column when the load is in tension.

The specimens are named as "WB(O/I drift ratio)-C(Maximum axial load ratio)T(Minimum axial load ratio)." When the number of minimum axial load ratio is not included, the specimen was under the constant axial load. The list of specimens can be seen in Table 4. Under the maximum compressive axial load, the ratios of shear capacity to flexural capacity are 0.48~0.49 in the in-plane direction, 1.67~1.72 in the out-of-plane direction. The capacities are calculated based on "Commentary on Structural Regulations of the Building Standard Law of Japan (2020)," which is referred to in practical structural design in Japan. Out-of-plane capacities are calculated as two columns ignoring the contribution of the wall panel.

The specimen WB15-C20T33 was repaired with cement mortar because it was not fully filled with concrete near the top of the test region. The material properties of the mortar are shown in Table 3.

Loading Protocol

The lateral loading path in the experiment is illustrated in Fig. 3. The first loading was out-of-plane lateral loading to the peak drifts (from [8] to [1]), and then in-plane lateral load was applied with keeping out-of-plane drift the same (from [1] to [2]). After reaching the peak point [2], the out-of-plane lateral load was unloaded and reloaded in the opposite direction until the out-of-plane drift became null (from [2] to [3]) and then the in-plane drift returned to 0 (from [3] to [4]). The loading procedure in the negative direction was the same as the positive one (from [4]

to [8]). The path from [1] to [8] in Fig. 3 was defined as one cycle. Two full cycles were applied with in-plane peak drifts of R_x=0.05, 0.10, 0.25, 0.50, 0.75, 1.00 and 2.00% rad.

Axial load varied depending on out-of-plane lateral load. In practical buildings, axial load on the wall with side columns varies not only with in-plane loading but also with out-of-plane loading. Axial load imposed on the specimens simulated this bi-directional loading effect in buildings. The relationship between axial load ratio and out-of-plane lateral load is shown in Fig. 4. In the figure, A_g is the gross sectional area of the shear wall, a_{cg} is the total sectional area of the longitudinal reinforcement of the side columns and ${}_{wo}Q_{mu}$ is the shear force when the out-of-plane flexural capacity under the maximum (compression) or minimum (tension) axial load. The axial load of $0.12A_g f'_c$ was first applied as the service load to the specimens WB15-C20T00, WB30-C20T00 and, WB15-C20T33, and then axial load varied depending on the out-of-plane lateral loading. Axial load increased or decreased linearly to the target values until lateral load reached half the out-of-plane flexural capacity ${}_{wo}Q_{mu}$. The target compressive axial load was $0.20A_g f'_c$, and the target tensile axial load was 0 for WB15-C20T00 and WB30-C20T00, or $-0.33a_{cg}f_y$ for WB15-C20T33.

Measurement Setup

Displacement transducers were attached to the loading block and the foundation block. Drift angle was obtained as the relative lateral displacement between the blocks, divided by the clear height of the wall (1400 mm). The load subjected to the specimen was measured with the load cells attached to the six jacks respectively.

Loading Setup

Loading setup is shown in Fig. 5. In-plane lateral load was applied by two 2000 kN-capacity jacks through steel frames that were connected to the specimen with PT bars. Cantilever moment distribution was assumed in the in-plane direction. A concrete block for loading was connected to the top of the specimen with PT bars. Out-of-plane horizontal and axial loads were applied to the loading block by two sets of 1000 kN-capacity jacks. Double-curvature moment distribution was assumed out-of-plane loading by keeping the top loading block horizontally by the vertical jacks.

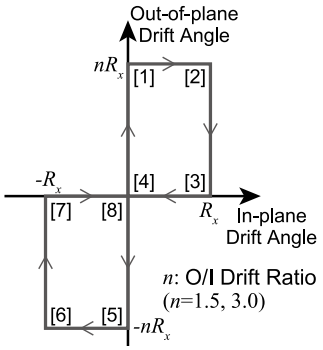

Figure 3. Lateral loading path

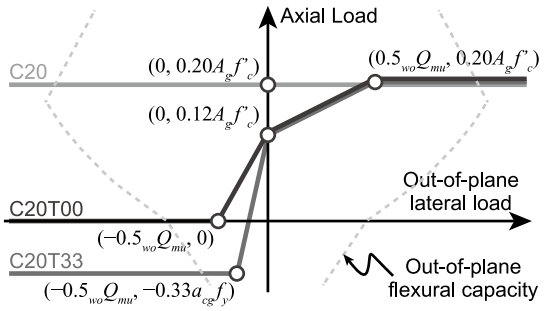

Figure 4. Loading path of axial load

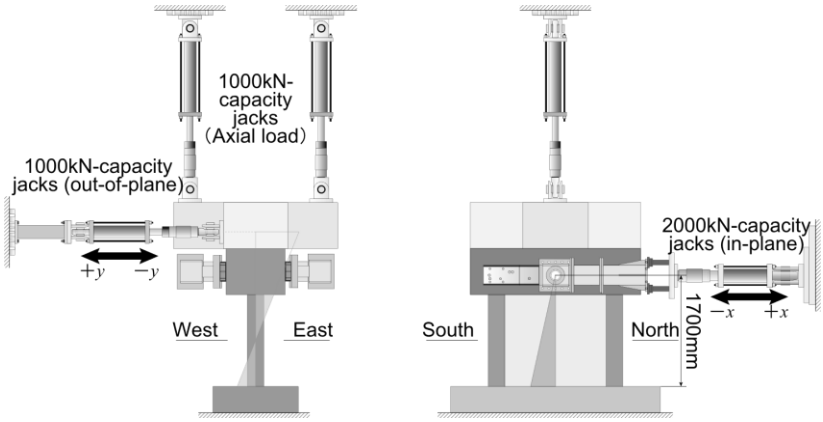

Figure 5. Loading setup

EXPERIMENTAL RESULTS

Lateral Load – Drift Angle Relationship

Figs. 6 and 7 show in-plane and out-of-plane hysteretic responses of each specimen, in which lateral load is plotted against horizontal drift angle. In the figures, the circle markers indicate the maximum load capacity. The white and black square markers indicate points when longitudinal reinforcements of the side columns yielded for the first time in tension or compression, respectively. The dashed lines indicate the ultimate shear capacity in the in-plane direction in Fig. 6, and the flexural capacity which includes the *P-Δ* effect in the out-of-plane direction in Fig. 7. The ultimate shear capacity is calculated with Equation (1). The flexural capacity is calculated with Equations (2) – (5). Equations (1) – (5) are cited from the commentaries of Japanese building design codes and enforcements (MLIT, 2020). The wall panel is not considered in out-of-plane flexural capacity. Only the flexural capacities of the side columns are included.

$$ {}_{wo}Q_{mu} = 2M_u / h_w \tag{2} $$

$$ M_{u1} = 0.5a_{cg}\sigma_{cy}g_1D + 0.5Ng_1D \qquad (N_{\min} \le N \le 0) \tag{3} $$

$$ M_{u2} = 0.5a_{cg}\sigma_{cy}g_1D + 0.5ND\left(1 - \frac{N}{bDf_c'}\right) \qquad (0 \le N \le N_b) \tag{4} $$

$$ M_{u3} = \left(0.5a_g\sigma_y g_1 D + 0.024(1+g_1)bD^2 f_c'\right)\left(\frac{N_{\max} - N}{N_{\max} - N_b}\right) \qquad (N_b \le N \le N_{\max}) \tag{5} $$

where
${}_{wo}Q_{mu}$ = out-of-plane shear force when out-of-plane flexural capacity;
M_u = out-of-plane flexural capacity;
h_w = out-of-plane shear span (= 700 mm);
f'_c = compressive strength of concrete;
a_{cg} = total cross sectional area of longitudinal reinforcements;
σ_{cy} = yield strength of longitudinal reinforcements;
g_1 = ratio of distance between gravity center of compressive reinforcements and one of tensile reinforcements to D;
b = column width;
D = column depth;
N = axial load;
$N_{\max} = bDf'_c + a_{cg}\sigma_{cy}$;
$N_{\min} = -a_{cg}\sigma_{cy}$; and
$N_b = 0.22(1+g_1)bDf'_c$.

For all specimens, during the first cycle for R_x=0.05%, shear cracks developed on the wall panel in both positive and negative directions of loading. Flexural cracks developed on the side columns during this cycle except for WB15-C20. This is because WB15-C20 was always subjected to high axial compressive load. During the R_x=0.10% cycle, new cracks developed, while widths of the existing cracks grew larger. It was in WB15-C20T33 that the longitudinal reinforcement of the side columns yielded in tension during the R_x=0.25% cycle. During the first cycle for R_x=0.50%, slight concrete crushing was observed at the top and bottom of the side columns and the wall panel. During this cycle, shear cracks appeared on the side columns. It seemed that the compression strut was damaged severely, and consequently the in-plane maximum load capacity was observed during this cycle. In this cycle, the longitudinal reinforcement yielded in compression, and compressive yielding occurred prior to tensile yielding except for WB15-C20T00.

(a) WB15-C20 with O/I drift ratio of 1.5 and constant axial load of $0.20A_gf'_c$
At the target drift angle of the first positive cycle for R_x=0.75%, concrete of the wall panel spalled off severely and in-plane loading was out of control. Consequently, the specimen deformed uncontrollably to R_x=0.97%, which was larger than the target deformation with capacity reduction as large as 70% of the maximum load-carrying capacity. The loading was terminated at the second cycle for R_x=0.75%.

(b) WB15-C20T00 with O/I drift ratio of 1.5 and varying axial load of 0 - $0.20A_gf'_c$
The specimen deformed to the larger drift angle than expected (about R_y=-3.7%) in the negative direction of the first cycle for R_x=2.00% because the displacement transducer did not function properly. Loading was carried on by using the transducer on the opposite side of the one in trouble.

(c) WB15-C20T33 with O/I drift ratio of 1.5 and varying axial load of -0.33$a_{cg}f'_y$ - 0.20$A_g f'_c$
At the deformation beyond R_x=0.75%, concrete of the wall panel spalled off in the positive direction more severely than in the negative direction of loading. Lateral load at the in-plane peak point [6] during the R_x=0.75% cycle was larger than the one during the R_x=0.50% cycle. From the peak point [8] to [1] in the second cycle for R_x=2.00%, the loading was stopped because the specimen was not able to sustain the axial load.

(d) WB30-C20T00 with O/I drift ratio of 3.0 and varying axial load of 0 - 0.20$A_g f'_c$
In the out-of-plane direction, stiffness and load capacity decreased severely after the R_x=0.75% cycle, and the maximum load capacity was attained during the first cycle for R_x=0.50%. On the other hand, in the negative direction in which axial load was in tension, severe concrete spalling was not observed until a new dominant shear crack developed during the R_x=1.00% cycle. Consequently, the maximum load capacity was observed during the first cycle for R_x=0.50%, and load capacity deterioration was more gradual than in the positive direction. From the peak point [6] to [7] in the first cycle for R_x=2.00%, the loading was stopped because the specimen was not able to sustain the axial load.

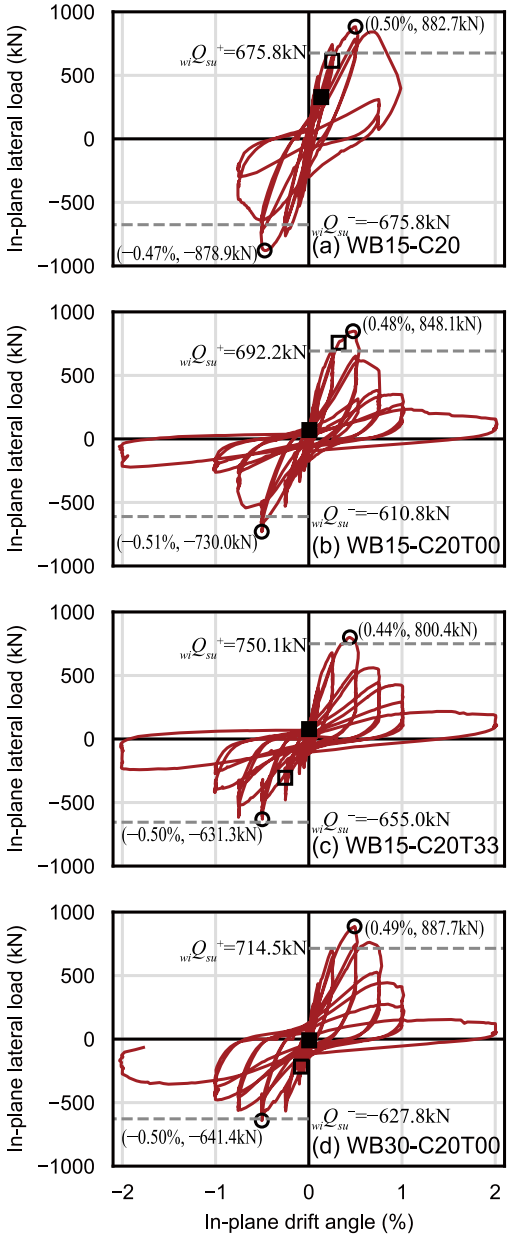

Figure 6. In-plane lateral load – drift angle relationships

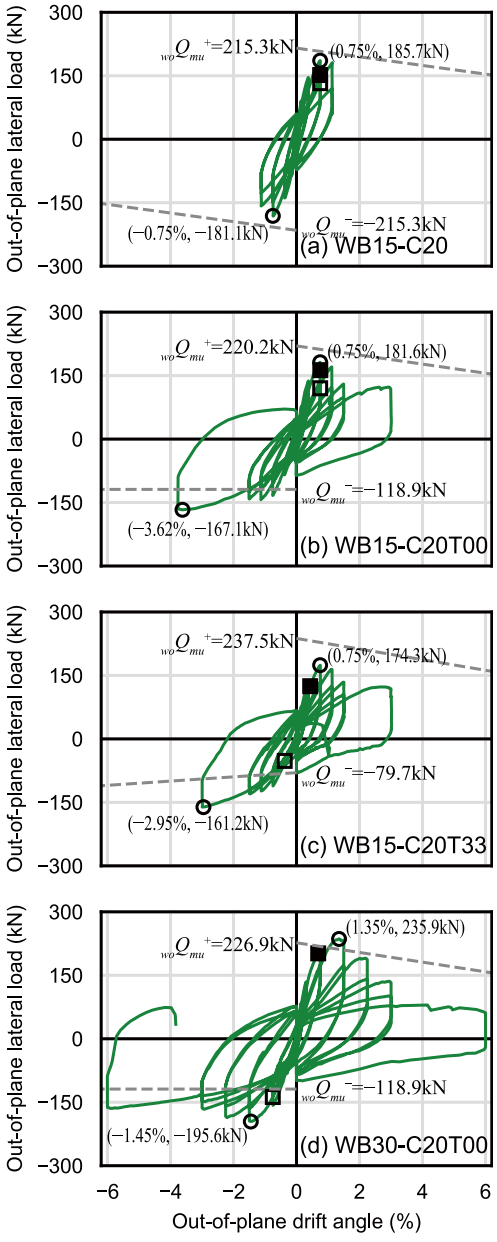

Figure 7. Out-of-plane lateral load – drift angle relationships

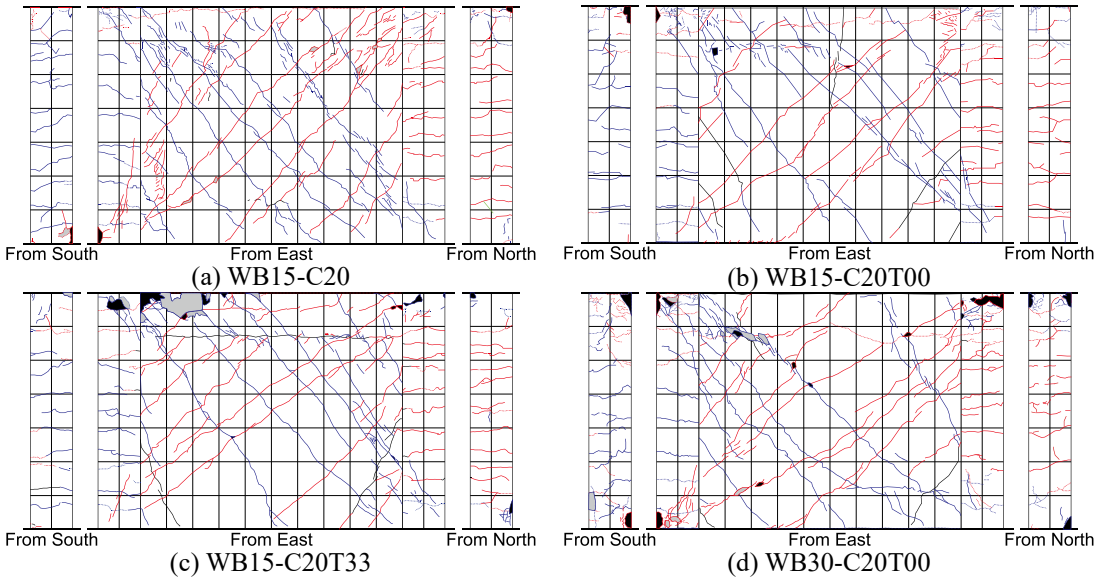

Figure 8. Cracks after completion of R_x=0.50% cycle

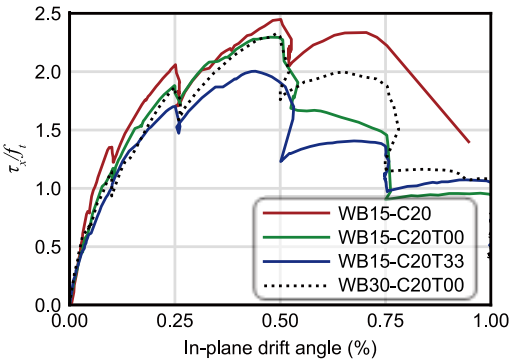

Figure 9. Envelope curve of in-plane lateral load – drift angle relationship

Table 5. Maximul load capcity under target axial load

Specimen		In-plane		Out-of-plane	
		$_{wi}Q_{max}$ (kN)	$_{wi}\tau_{max}/f_t$	$_{wo}Q_{max}$ (kN)*	$_{wo}\tau_{max}/f_t$
WB15-C20	+	882.7	2.448	185.7	0.515
	−	-878.9	-2.437	-181.1	-0.502
WB15-C20T00	+	841.7†	2.278	181.6	0.491
	−	-651.7†	-1.764	-167.1	-0.452
WB15-C20T33	+	800.4	2.003	174.3	0.436
	−	-525.4†	-1.315	-161.2	-0.403
WB30-C20T00	+	887.7	2.327	235.9	0.619
	−	-590.3†	-1.548	-195.6	-0.513

*Includes contribution of additive bending by *P-Δ* effect,
†Mismatches the maximum load capacity in Figure 6.

Damage Progress

Fig. 8 shows cracks observed after the R_x=0.50% cycle. In the figure, the blue lines indicate cracks observed at the point [1], [2] or [3] in Fig. 3, the red lines indicate cracks observed at the point [5], [6] or [7], and the dashed lines indicate cracks observed after out-of-plane loading, point [1] or [5]. The gray region indicates areas with concrete spalling, and the black region indicates concrete peeling off.

In every specimen, shear cracks were observed on the side columns at the R_x=0.50% cycle. Furthermore, at the south top area of the wall panel, fine cracks appeared as a sign of concrete crushing, and concrete spalled off at this cycle. Therefore, it appeared that the maximum load capacity was determined by the crushing of the compression strut. WB15-C20T33 had a larger spalling area than the other specimens did at the R_x=0.50% cycle. This is because concrete at the top region was weaker than in the bottom region due to upright concrete casting. WB30-C20T00 had larger concrete spalling or peeling area on the side columns than WB15-C20T00 did. Damages observed in the wall panels of WB30-C20T00 and WB15-C20T00 were similar.

Except for WB15-C20 whose loading was stopped at the R_x=0.75% cycle, the tests were stopped at the R_x=2.00% cycle. Judging from dominant shear cracks, the width of the compression strut appeared to be smaller when axial load was in tension than in compression. Difference in stress transfer mechanisms was apparent when the axial load varied from tension to compression and vice versa. These mechanisms need to be studied further. WB15-C20T33 had damage concentrated in the top region of the wall segment because of weaker concrete caused by upright concrete casting.

Maximum Load Capacity and Envelope Curve

Maximum load capacities under target axial load are summarized in Table 5. There are cases in which these maximum load capacities do not match those in Fig. 6. This is because the maximum load capacities in Fig. 6 were not always attained under target axial load. In the table, the normalized shear stresses obtained as shear stress τ divided by concrete tensile strength f_t are listed. The shear stress τ is obtained as the lateral load Q divided by the horizontal gross cross-sectional area A_g. The concrete tensile strength f_t is calculated with Equation (6). The envelope curve of in-plane normalized shear stress τ_x/f_t – in-plane drift angle relationships are shown in Fig. 9.

$$f_t = 0.33\sqrt{f_c'} \tag{6}$$

where f'_c = compressive strength of concrete (MPa).

(a) In-plane
Comparison among the three specimens WB15-C20, WB15-C20T00 and WB15-C20T33 whose O/I drift ratio is 1.5 showed the tendency that the bigger difference between the maximum and minimum axial loads was, the lower maximum load capacity was attained. The same trend was observed for the normalized shear stress τ_x/f_t in Fig. 9 up to the maximum load capacity. A factor that lowered the maximum load capacity appears to be yielding of longitudinal reinforcements and concrete damage of the side columns.

Comparison between WB15-C20T00 and WB30-C20T00, whose difference was O/I drift ratio only, did not show significant difference in both maximum load capacities and envelope curves of τ_x/f_t. This trend does not match the trend that the lower in-plane maximum load capacity is obtained, the larger O/I drift ratio was, which is a conclusion derived from loading tests in past research (Idosako et al., 2017). Furthermore, the authors' analytical investigation (Yamada et al., 2019) using FEM on shear walls with constant axial load of 0.20 also contradicts the conclusion in Idosako's research.

(b) Out-of-plane
Comparison among the three specimens WB15-C20, WB15-C20T00 and WB15-C20T33 whose O/I drift ratio is 1.5 revealed that the bigger difference between the maximum and minimum axial loads was, the lower maximum load capacity was observed as in the in-plane direction. The normalized shear stress of WB15-C20T33 was 15% lower than that of WB15-C20. It appears to be concrete spalling off due to the tensile axial load that affected the ultimate flexural capacity.

Comparison between WB15-C20T00 and WB30-C20T00, whose difference was O/I drift ratio only, revealed that WB30-C20T00 with the larger O/I drift ratio had 30% higher maximum load capacity and 26% higher normalized shear stress than WB15-C20T00 did. This is due to the out-of-plane drift angle R_y for which the maximum load capacity was observed. The out-of-plane maximum load capacity occurred at R_y=0.75% for WB15-C20T00, and at R_y=1.35% for WB30-C20T00, which corresponds the R_x=0.50% cycle. In this cycle, shear cracking due to in-plane deformation occurred also in the side columns, and the damage is assumed to have affected the out-of-plane maximum load capacity.

Shear Deformation and Flexural Deformation

The variation of shear and flexural stiffness was analyzed by deformation decomposition to study the effect of loading conditions on the in-plane resistance mechanism. The location of displacement transducers used for the deformation decomposition is shown in Fig. 10. The shear deformation and the flexural deformation are calculated with Equations (7) and (8).

$$u_s = \frac{\sqrt{H^2 + L^2}}{L} \cdot \frac{\delta_4 - \delta_3}{2} \tag{7}$$

$$u_f = \frac{H}{2L}(\delta_1 - \delta_2) \tag{8}$$

where
u_s = shear deformation;
u_f = flexural deformation; and
H, L, δ_1, δ_2, δ_3 and δ_4 are indicated in Fig. 10.

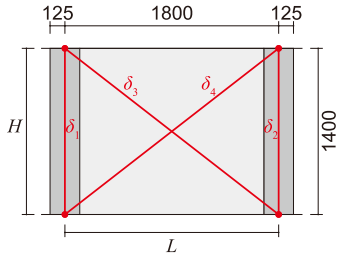

Figure 10. Location of displacement transducers to separate deformation (unit: mm)

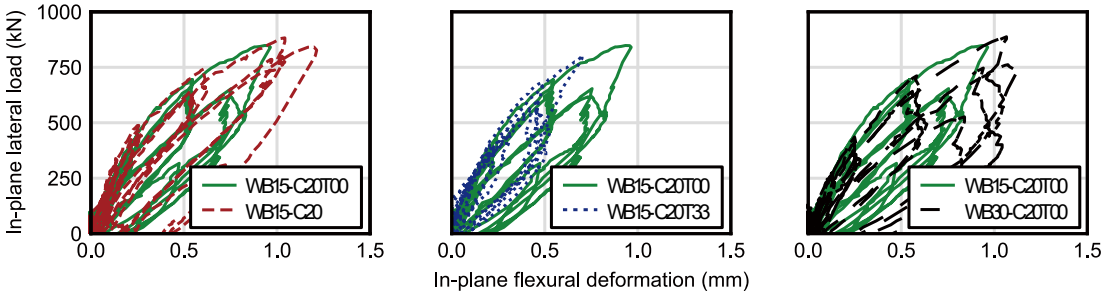

Figure 11. In-plane lateral load - flexural deformation relationships

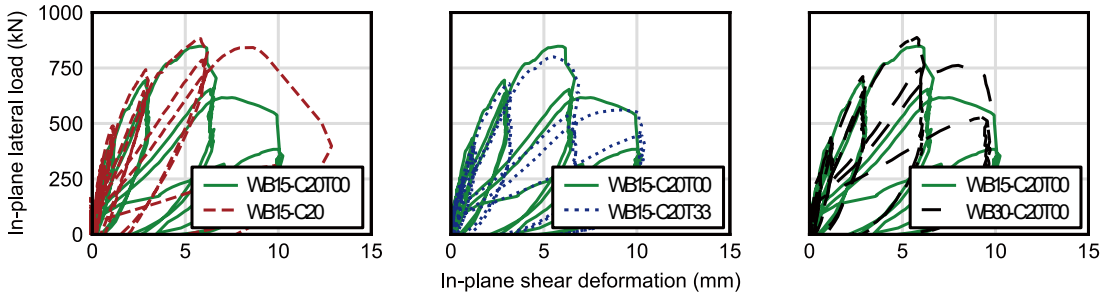

Figure 12. In-plane lateral load - shear deformation relationships

Figs. 11 and 12 show relationships between decomposed flexural and shear deformation and in-plane lateral load, respectively. Compared with WB15-C20T00, WB15-C20 had no significant difference in the amount of flexural deformation up to the maximum load capacity. However, it was only WB15-C20 that showed an increase in flexural deformation after the maximum load capacity was attained. Similarly, the flexural deformation of WB30-C20T00 after the maximum load capacity was reached was larger than that of WB15-C20T00. On the other hand, the flexural deformation of WB15-C20T33 was smaller than that of the other specimens even before the maximum load capacity was attained. There was no significant difference in the amount of shear deformation in each cycle up to the R_x=0.75% cycle for all specimens.

Although a simple comparison cannot be made because of the effect of material strength, the axial force variation and the out-of-plane deformation do not seem to have a significant effect on the shear stiffness. On the other hand, the flexural stiffness of WB30-C20T00 only seemed to be slightly decreased.

CONCLUSIONS

In this paper, loading test was conducted on reinforced concrete shear walls to study the effects of varying axial load and out-of-plane deformation on their structural performance. Obtained findings are listed below.

- The bigger difference between the maximum axial load and the minimum axial load was, the lower maximum load capacity the specimen showed.
- Out-of-plane deformation did not affect in-plane maximum load capacity. This tendency did not match the trend which was shown in past research (Idosako et al., 2017).
- The ratio of the out-of-plane maximum load capacity to the calculated out-of-plane flexural capacity was less than 1.00 under high compressive axial load for the specimens whose O/I drift ratio was 1.5. This is because shear cracks appeared on the side columns due to the in-plane deformation before the specimens reached the out-of-plane flexural load capacity.

ACKNOWLEDGEMENTS

This research was financially supported by JSPS KAKENHI, Grant Numbers JP18H01586 (Principal Investigator: M. Nishiyama). Haikou Onoda Ready Mixed Concrete Co. Ltd., and M. Nomura, Kyoto University technical staff, gave us many helps to conduct experiment. K. Sugimoto (Yokohama National University) and M. Sakashita (Building Research Institute) gave us a lot of advice. The authors express gratitude for their support.

REFERENCES

A. Niroomandi, S. Pampanin, R.P. Dhakal, M. Soleymani Ashtiani and C. de la Torre (2018), "Rectangular RC Walls under Bi-directional Loading: Recent Experimental and Numerical Findings," *Proceedings of New Zealand Concrete Industry Conference*, Hamilton, New Zealand.

K. Beyer, A. Dazio, and M. J. N. Priestley (2008), "Quasi-static cyclic tests of two U-shaped reinforced concrete walls," *Journal of Earthquake Engineering*, vol. 12, no. 7, pp. 1023-1053.

K. Kusunoki et al (2019), "Study on the Accuracy of Practical Functions for R/C Wall by a Developed Database of Experimental Test Results," *Bulletin of Earthquake Engineering*, 17, pp. 6621-6644.

K. Sugimoto et al. (2017), "Collapse Behavior of 6 Story Wall Frame Building During Shaking Table Test, Research and Development for Quantification of Collapse Margin of RC Buildings," *Journal of Structural and Construction Engineering (Transactions of AIJ)*, Japan, V. 82, No. 741, pp. 1759-1768

K. Yonezawa et al. (2018), "Nonlinear FE Analysis for Shaking Table Test of RC 6 Story Building, Research and Development for Quantification of Collapse Margin of RC Buildings," *Journal of Structural and Construction Engineering (Transactions of AIJ)*, Japan, V. 83, No. 746, pp. 589-599

Ministry of Land, Infrastructure and Transport (MLIT) et al. (2020), "Kenchikubutsu no Kouzou Gijutsu Kijun Kaisetsusho (Commentary on Structural Regulations of the Building Standard Law of Japan)" (in Japanese)

R. Yamada, M. Tani, M. Nishiyama (2019), "Analytical Study on Effect of Bi-directional Lateral Loading and Axial Loading on Structural Performance of R/C Shear Walls by Finite Element Analysis," *Proceedings of The 21st Taiwan-Korea-Japan Joint Seminar on Earthquake Engineering for Building Structures*, pp.156-165

T. Kawai et al. (2016), "Effect of Construction Joint and Axial Load on Slip Behavior of RC Shear Wall," *Proceedings of Tokai Chapter Architectural Research Meeting*, Japan, V. 54, pp. 189-192 (in Japanese)

Y. Idosako, M. Sakashita, M. Tani, and M. Nishiyama (2017), "Bi-directional Lateral Loading Tests on RC Shear-dominant Walls," *Journal of Structural and Construction Engineering (Transaction of AIJ)*, Vol. 735, 683-692 (in Japanese)